A theoretical study of the atomic and electronic structure of a grain boundary in cubic SiC



1990 J. Phys.: Condens. Matter 2 7809

(http://iopscience.iop.org/0953-8984/2/38/007)

J. Phys.: Condens. Matter 2 (1990) 7809–7823. Printed in the UK

# A theoretical study of the atomic and electronic structure of a grain boundary in cubic SiC

M Kohyama†, S Kose†, M Kinoshita† and R Yamamoto‡

† Glass and Ceramic Material Department, Government Industrial Research Institute, Osaka, 1-8-31 Midorigaoka, Ikeda, Osaka 563, Japan

‡ Research Center of Advanced Science and Technology, University of Tokyo, 4-6-1 Komaba, Meguro-ku, Tokyo 153, Japan

Received 2 January 1990

**Abstract.** The atomic and electronic structure of the $\{1\,2\,2\}\,\Sigma = 9$ grain boundary in cubic SiC has been calculated for the first time using the self-consistent tight-binding (SCTB) method. An atomic model consisting of a zig-zag arrangement of five-membered and seven-membered rings similar to that in the same boundary in Si or Ge has been constructed from a high-resolution electron microscope image, although Si–Si and C–C wrong bonds are repeated alternately at the interface in this model. We have also performed calculations of the same boundary in Si using the SCTB method for comparison, and have obtained results similar to those previously obtained by other theoretical schemes. The calculated boundary energy in SiC has shown that the present atomic model can exist stably compared with the two surfaces, and the calculated boundary electronic structure in SiC has no deep states in the gap as well as that in Si. These results indicate the possibility that stable boundary structures can be constructed by arranging structural units in SiC as well as in covalent semiconductors. However, it has been found that the presence of the wrong bonds greatly influences the boundary energy and the boundary electronic structure. The increase in the electrostatic energy caused by the wrong bonds is a large part of the present boundary energy in SiC, differently from that in Si, and it has been shown that the wrong bonds introduce the wrong-bond localised states at the band edges and within the valence band.

## 1. Introduction

Various properties of ceramics such as sintering, mechanical and electronic properties depend on grain boundaries. It is of much importance to understand the structures and properties of grain boundaries in ceramics from a microscopic viewpoint. Nowadays, it is possible to obtain experimentally valuable information about atomic structures of grain boundaries in ceramics by virtue of recent developments in the technique of electron microscopy [1–4]. On the other hand, recent developments and improvements in theoretical schemes and high-performance computers have made possible theoretical approaches to atomic structures and properties of grain boundaries in ceramics. However, these theoretical approaches have been carried out only for grain boundaries in ionic ceramics such as MgO and NiO [5–7]. It is necessary to deal with grain boundaries in covalent ceramics such as SiC and $Si_3N_4$ theoretically. In these systems, it is essential to calculate electronic structure at the interface.

0953-8984/90/387809 + 15 $03.50 

On the other hand, significant advances have been made in the understanding of atomic and electronic structures of grain boundaries in covalent semiconductors such as Si and Ge. From various observations [8–10] and theoretical calculations [11–15], it has been shown that frequently observed coincident site lattice (CSL) boundaries such as the $\{1\,1\,1\}$ $\Sigma = 3$, the $\{2\,1\,1\}$ $\Sigma = 3$, the $\{1\,2\,2\}$ $\Sigma = 9$ and the $\{2\,5\,5\}$ $\Sigma = 27$ boundaries are constructed by arranging structural units such as five-membered rings and seven-membered rings and are electrically non-active because of dangling-bond reconstruction at interfaces. It is interesting to examine whether these features of grain boundaries in covalent semiconductors are applicable to grain boundaries in covalent ceramics or not.

In this paper, we have constructed an atomic model of the $\{1\,2\,2\}\Sigma = 9$ grain boundary (second-order twin boundary) in $\beta$-SiC and calculated theoretically the stable atomic configuration, boundary energy and electronic structure for the first time. The results have been compared with those of the same type of boundary in Si.

## 2. Atomic model

Hiraga has obtained a high-resolution electron microscope (HREM) image of the $\{1\,2\,2\}$ $\Sigma = 9$ grain boundary in chemical vapour-deposited (CVD) $\beta$-SiC [1]. He has found that there exist coherent matching and periodic structure at the interface. By comparing this image with a HREM image of the same type of boundary in Ge [9], we have found that there is a great similarity between the two images. It has already been shown that the $\{1\,2\,2\}$ $\Sigma = 9$ grain boundary in Si or Ge has a reconstructed structure where a zig-zag arrangement of two sets of five-membered and seven-membered rings constitutes one period along the $\langle 4\,1\,1\rangle$ direction in projection onto the $\{0\,1\,1\}$ plane [8, 9, 11, 12]. We call one set of five-membered and seven-membered rings a 5–7 unit [16]. A similar atomic model consisting of a zig-zag arrangement of 5–7 units can also be constructed for the $\{1\,2\,2\}$ $\Sigma = 9$ boundary in $\beta$-SiC. Recently, Hagège *et al* [17] have used image simulation and found that this type of model can explain the HREM image [1].

However, odd-membered rings in SiC introduce wrong bonds between like atoms, and it is possible to construct three types of model of this boundary with respect to the kinds of wrong bond. One contains only C–C wrong bonds, another contains only Si–Si wrong bonds and the other contains both C–C and Si–Si wrong bonds at the interface. The former two models have glide-plane symmetry with respect to the interface as well as the model in Si or Ge, and are expressed as $p2_1^1ma'$ [18]. However, the last model does not have glide-plane symmetry but only mirror symmetry with respect to the $\{0\,1\,1\}$ plane and is expressed as *pm*. This is because one of the two grains constituting the interface is inverted in this model as compared with the former two models. In this model, Si–Si wrong bonds and C–C wrong bonds are repeated alternately at the interface and the two sets of 5–7 units constituting one period along the $\langle 4\,1\,1\rangle$ direction are not similar to each other. It seems that the HREM image of this boundary in SiC [1] does not have glide-plane symmetry strictly by a small rigid-body translation along the $\langle 4\,1\,1\rangle$ direction, which supports the presence of the last model, although further precise observations are needed in order to settle this problem completely.

In this paper, as the first step, we treat the last model. We have calculated the boundary energy, the stable atomic configuration and the electronic structure of this model quantum-mechanically.

## 3. Method of calculation

*Ab initio* calculations are formidable tasks in the present case because of the large number of non-equivalent atoms. The tight-binding electronic theories [19, 20] have been shown to be quite useful for calculations of grain boundaries in covalent semiconductors [11–15]. However, for calculations of lattice defects in solids with both properties of covalency and ionicity such as SiC, it is necessary to incorporate the effects of self-consistent charge redistribution and electrostatic interactions, which cannot be included in the usual tight-binding theories. Thus we have used the self-consistent tight-binding (SCTB) method [21–23]. The SCTB method can deal with covalency and ionicity on an equal footing, and is capable of calculating electronic structure, total energy and atomic forces sufficiently rapidly for the lattice relaxation of extended defects as well as other tight-binding methods. Results can be easily analysed and can give a simple chemical picture as compared with the *ab initio* methods.

The precise description of the present method has been given in our preceding paper [23]. The essence of this method can be described as follows. The orthogonalised basis functions are constructed as

$$|i\alpha, \boldsymbol{k}\rangle = N^{-1/2} \sum_{\boldsymbol{R}} \exp[\mathrm{i}\boldsymbol{k} \cdot (\boldsymbol{t}_i + \boldsymbol{R})] \varphi_{i\alpha}(\boldsymbol{r} - \boldsymbol{t}_i - \boldsymbol{R}) \tag{1}$$

where $\varphi_{i\alpha}(\boldsymbol{r} - \boldsymbol{t}_i - \boldsymbol{R})$ is the $\alpha$th atomic orbital centred on an atom $i$ located at $\boldsymbol{t}_i + \boldsymbol{R}$, $\boldsymbol{R}$ is a lattice vector representing each unit cell of the periodic system and $N$ is the number of unit cells in the system. The eigenfunction of the tight-binding Hamiltonian with wavevector $\boldsymbol{k}$ and band index $n$ is expressed as

$$|n, \boldsymbol{k}\rangle = \sum_{i\alpha} C_{i\alpha}^{n\boldsymbol{k}} |i\alpha, \boldsymbol{k}\rangle. \tag{2}$$

The effects of the charge transfer between atoms and the overlap between local atomic orbitals are included in the on-site elements of the Hamiltonian as

$$E_{i\alpha} = E_{i\alpha}^0 + U_i(Q_i - Z_i) + P_i + f_{i\alpha}. \tag{3}$$

The first term is the orbital energy of the neutral free atom $i$. The second term expresses the change in the intra-atomic Coulomb potential. $U_i$ is an average of the intra-atomic Coulomb integrals of the valence electrons of the atom $i$. $Z_i$ and $Q_i$ are the charge of the ion core and the self-consistent occupancy of the atom $i$. $Q_i$ is given by

$$Q_i = \sum_{\alpha} Q_{i\alpha} = \sum_{\alpha} \sum_{n,\boldsymbol{k}}^{\mathrm{occ}} C_{i\alpha}^{n\boldsymbol{k}^*} C_{i\alpha}^{n\boldsymbol{k}}. \tag{4}$$

The third term in equation (3) is the inter-atomic electrostatic potential for an electron located on the atom $i$ and is given by

$$P_i = (Q_i - Z_i)\Phi_0 + \sum_{j \neq i} (Q_j - Z_j)\Phi_{ij} \tag{5}$$

where

$$\Phi_0 = \sum_{\boldsymbol{R} \neq 0} V(\boldsymbol{R})$$

and

$$\Phi_{ij} = \sum_{\boldsymbol{R}} V(\boldsymbol{t}_j + \boldsymbol{R} - \boldsymbol{t}_i).$$

Here $j$ indicates the atoms other than $i$ in the unit cell. $V(\boldsymbol{r}_j - \boldsymbol{r}_i)$ is an effective inter-atomic electrostatic function, which expresses a simple Coulomb potential for large

distances and includes the effects of charge overlap for short distances. The fourth term in equation (3) is the non-orthogonality correction and is given by the overlap matrix elements between atomic orbitals as

$$f_{i\alpha} = -\sum_{j\beta} H_{i\alpha j\beta} S_{j\beta i\alpha}. \tag{6}$$

By solving the above one-electron Schrödinger equation self-consistently, the band-structure energy $E_{\rm bs}$ is given as a sum of the eigenenergies of occupied states. The total energy $E_{\rm tot}$ is given by subtracting the doubly counted electron–electron electrostatic energy and adding the ion–ion electrostatic energy. The binding energy $E_{\rm B}$ per unit cell, which is the difference between the total energy of the system and that of the free atoms, $E^0_{\rm atom}$, can be written as a sum of the following four terms:

$$E_{\rm B} = E_{\rm pro} + E_{\rm Mad} + E_{\rm ov} + E_{\rm cov} \tag{7a}$$

where

$$E_{\rm pro} = \sum_i \left( \sum_\alpha Q_{i\alpha}(E^0_{i\alpha} - U_i Z_i) + \tfrac{1}{2} U_i Q_i^2 \right) - E^0_{\rm atom} \tag{7b}$$

$$E_{\rm Mad} = \tfrac{1}{2} \sum_i (Q_i - Z_i) P_i$$

$$= \tfrac{1}{2} \sum_i (Q_i - Z_i)^2 \Phi_0 + \tfrac{1}{2} \sum_i \sum_{j \neq i} (Q_i - Z_i)(Q_j - Z_j) \Phi_{ij} \tag{7c}$$

$$E_{\rm ov} = \sum_{i\alpha} Q_{i\alpha} f_{i\alpha} \tag{7d}$$

and

$$E_{\rm cov} = E_{\rm bs} - \sum_{i\alpha} Q_{i\alpha} E_{i\alpha}$$

$$= \sum_{n,\boldsymbol{k}}^{\rm occ} \sum_{i\alpha} \sum_{j\beta} C^{n\boldsymbol{k}*}_{i\alpha} C^{n\boldsymbol{k}}_{j\beta} \sum_{\boldsymbol{R}} \exp[{\rm i}\boldsymbol{k}\cdot(\boldsymbol{t}_j + \boldsymbol{R} - \boldsymbol{t}_i)] H_{\alpha\beta}(\boldsymbol{t}_i, \boldsymbol{t}_j + \boldsymbol{R}) \tag{7e}$$

where $H_{\alpha\beta}(\boldsymbol{t}_i, \boldsymbol{t}_j + \boldsymbol{R})$ is the inter-atomic Hamiltonian element between $\varphi_{i\alpha}(\boldsymbol{r} - \boldsymbol{t}_i)$ and $\varphi_{j\beta}(\boldsymbol{r} - \boldsymbol{t}_j - \boldsymbol{R})$. $E_{\rm pro}$ contains the promotion energy, the energy gain by electron transfer between different kinds of atoms and the change in the intra-atomic electrostatic energy between electrons. $E_{\rm Mad}$ is the inter-atomic electrostatic energy (Madelung energy), which is a sum of interactions between effective charges of respective atoms, $Q_i - Z_i$. $E_{\rm ov}$ is the overlap interaction energy, which expresses the increase in the kinetic energy of the electrons upon compression. This term is often given by a simple sum of inter-atomic potentials in usual tight-binding theories [19, 20]. $E_{\rm cov}$ is the covalent energy and contains only the contribution from the inter-atomic covalent bonding.

Atomic forces are also given very easily [22, 23] via the Hellmann–Feynman theorem as well as other tight-binding theories [19, 20], and lattice relaxation can be performed easily.

We have used the following parameters and functional forms in the SCTB method determined so as to reproduce the basic properties of $\beta$-SiC, Si and C adequately in our preceding paper [23]. One s and three p valence orbitals per atom are included in the

**Table 1.** Parameters used in the calculations [21]†.

| | Si | C |
|---|---|---|
| $E_s^0$ (eV) | −14.68 | −19.19 |
| $E_p^0$ (eV) | −8.08 | −11.79 |
| $U$ (eV) | 7.64 | 11.76 |
| $\eta_{ss\sigma} = -1.38$ | $\eta_{s_ap_c\sigma} = 1.68$ | $\eta_{s_cp_a\sigma} = 1.92$ |
| $\eta_{pp\sigma} = 2.20$ | $\eta_{pp\pi} = -0.55$ | |

† In the universal tight-binding parameters, a and c denote anion and cation. For elemental solids or wrong bonds, the average is used.

basis set. The two-centre integrals of the Hamiltonian are expressed by assuming the $r^{-2}$ dependence on the inter-atomic distance $r$ as

$$H_{ll'm} = \eta_{ll'm}\hbar^2/mr^2. \tag{8}$$

The universal tight-binding parameters $\eta_{ll'm}$ [21, 24] are listed in table 1. The energy levels of free atoms and the intra-atomic Coulomb repulsions in equation (3) are also listed. For the effective inter-atomic electrostatic function, we have used the following form [21]:

$$V(\boldsymbol{r}_j - \boldsymbol{r}_i) = \frac{e^2}{|\boldsymbol{r}_j - \boldsymbol{r}_i|} - \frac{e^2}{|\boldsymbol{r}_j - \boldsymbol{r}_i|}\exp\left(-\frac{U_{Si} + U_C}{2}\frac{|\boldsymbol{r}_j - \boldsymbol{r}_i|}{e^2}\right). \tag{9}$$

The two-centre overlap integrals used in equation (6) have a $p/r^4 + q$ form as

$$S_{ll'm} = \eta_{ll'm}[2/(E_{il}^0 + E_{jl'}^0)](\hbar^2/m)(p/r^4 + q). \tag{10}$$

This form has been found so as to reproduce the bond lengths, binding energies and bulk moduli of all Si, $\beta$-SiC and C adequately [23]. This form is more favourable than a $1/r^3$ form [21] or a $1/r^2$ form for a system containing wrong bonds because this form can reproduce the thermodynamic stability condition of SiC for Si and C, although this form is improper for largely distorted systems as shown in our preceding paper [23]. Parameters $p$ and $q$ have been determined so as to reproduce the experimental bond length and the experimental binding energy for $\beta$-SiC, Si and C, respectively, and are listed in table 2. For Si–Si wrong bonds and C–C wrong bonds in SiC, we have used the values for Si and C, respectively.

All the calculations of the present grain boundary using the above SCTB method are carried out with use of the supercell technique. In this technique, in addition to the two-dimensional periodicity parallel to the boundary plane, periodicity normal to the boundary plane is imposed by stacking symmetric boundary planes alternately. Thus

**Table 2.** Parameters for the overlap integrals [23].

| | SiC | Si | C |
|---|---|---|---|
| $p$ (Å$^2$) | 0.4244 | 0.6883 | 0.2988 |
| $q$ (Å$^{-2}$) | 0.0635 | 0.0214 | 0.1586 |

**Table 3.** Calculated energy values of the {122} $\Sigma = 9$ grain boundaries in $\beta$-SiC and Si. Energy increases per supercell against the values in the perfect crystals are shown. Each supercell contains two symmetric interfaces in the present calculations. $E_{gb}$ is the interfacial energy per unit area for one interface.

| | Si | | $\beta$-SiC | |
|---|---|---|---|---|
| | 80-atom cell | 144-atom cell | 80-atom cell | 144-atom cell |
| $\Delta E_{pro}$ (eV/cell) | 0.283 | 0.274 | −1.785 | −1.785 |
| $\Delta E_{Mad}$ (eV/cell) | −0.008 | −0.008 | 4.022 | 4.021 |
| $\Delta E_{ov}$ (eV/cell) | 2.410 | 2.345 | 7.756 | 7.645 |
| $\Delta E_{cov}$ (eV/cell) | −0.829 | −0.762 | −4.915 | −4.808 |
| $\Delta E_{B}$ (eV/cell) | 1.856 | 1.849 | 5.079 | 5.072 |
| $E_{gb}$ (J m$^{-2}$) | 0.336 | 0.335 | 1.427 | 1.425 |

it is possible to utilise a conventional method of band-structure calculation with respect to a large unit cell containing two symmetric interfaces. For the present model of the {122} $\Sigma = 9$ boundary in $\beta$-SiC, the supercell structure is orthorhombic and belongs to the point group $C_{2v}$.

It is desirable that the distance between two neighbouring boundary planes is sufficiently large. In the present calculations, both 80-atom and 144-atom supercells have been used in order to examine the dependence on the size of the cell. The distances between the two neighbouring boundary planes in the two supercells of SiC are about 15 Å and 26 Å respectively. The optimum rigid-body translation between the two grains was determined by iterating lattice relaxation of the 80-atom cell for various translations. The same translation was used for the lattice relaxation of the 144-atom cell.

The number of special $\boldsymbol{k}$-points and the ranges of lattice sums in real and reciprocal space in the Ewald method for calculation of equation (5) were determined by supercell calculations of the perfect crystal with the same size and the same periodicity as the supercells of the boundary. In each step of lattice relaxation, the self-consistent iteration was terminated if the differences between input and output occupancies of respective atoms are all kept within a given tolerance ($10^{-5}$ electrons).

In addition to the calculations of the boundary in $\beta$-SiC, we have also performed calculations for a similar atomic model of the same type of boundary in Si using the same theoretical method for comparison. This structure in Si has already been examined by other theoretical schemes [11, 12].

## 4. Grain boundary energy and atomic structure

Table 3 shows the calculated energy values. All the values are the differences from those in the perfect crystals. Figures 1 and 2 show the calculated stable atomic configurations and the self-consistent effective charges of respective atoms, $-(Q_i - Z_i)$, in the 144-atom cells of Si and $\beta$-SiC. As shown in table 3, the dependence on the size of the supercell is not very large and the values of the 144-atom cells can be regarded as converged ones. This is true of the atomic configurations and effective charges.

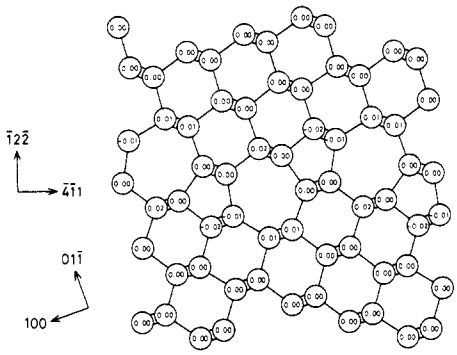


**Figure 1.** Relaxed atomic structure of the {122} $\Sigma = 9$ grain boundary in Si. Atomic positions are projected along the [011] axis. The numbers inside the circles indicate the effective charges of respective atoms, $-(Q_i - Z_i)$, expressed in units of $e$.

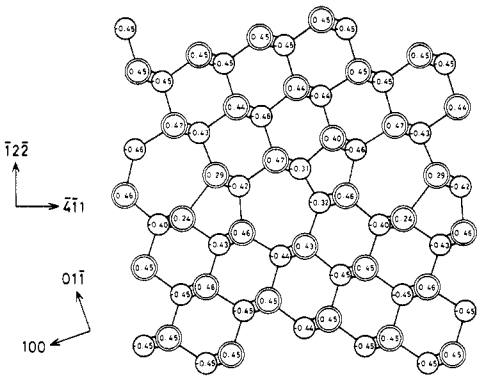


**Figure 2.** Relaxed atomic structure of the {122} $\Sigma = 9$ grain boundary in $\beta$-SiC. Atomic positions are projected along the [011] axis. The circles and the double circles indicate C atoms and Si atoms, respectively. The numbers inside the circles indicate the effective charges of respective atoms, $-(Q_i - Z_i)$, expressed in units of $e$. The effective charges in the perfect crystal are $\pm 0.45e$.

The calculated boundary energy per unit area of the {122} $\Sigma = 9$ boundary in Si is comparable with the values of 0.32 and 0.29 J m$^{-2}$ calculated using the semi-empirical tight-binding (SETB) method [11] and the density-functional theory [12]. This means the present SCTB method is reliable. For the boundary energy of SiC, we can conclude that the present model of the {122} $\Sigma = 9$ boundary in $\beta$-SiC possibly exists stably as compared with the estimated values of the surface energies of SiC [25].

The optimum rigid-body translation between the two grains of Si in figure 1 is $\boldsymbol{t}_\perp = 0.005a_0[\bar{1}2\bar{2}]$, which is a slight dilatation along the $[\bar{1}2\bar{2}]$ direction. This component is defined compared with a structure where the distance between neighbouring $(\bar{1}2\bar{2})$ atomic planes at the interface is set to that in the perfect crystal. On the other hand, in the case of SiC in figure 2, the structure of the interface does not have glide-plane symmetry and the optimum rigid-body translation has two components: $\boldsymbol{t}_\perp = 0.005a_0[\bar{1}2\bar{2}]$ and $\boldsymbol{t}_\parallel = 0.01a_0[\bar{4}\bar{1}1]$. These components are also defined compared with a structure similar to that in Si with glide-plane symmetry. The latter component is not contained in the periodic vectors of the supercell geometry because these types of component of the two symmetric interfaces in one supercell offset each other. Thus this component is determined from the relaxed atomic configuration itself. As shown in figure 2, it can be said that the translation along the $[\bar{4}\bar{1}1]$ direction is caused mainly by the difference between the bond lengths of a C–C wrong bond and a Si–Si wrong bond at the interface.

In the stable atomic configuration of the grain boundary in Si shown in figure 1, the bond-length deviations from that in the perfect crystal range from $-1.9\%$ to $1.5\%$ and the bond-angle deviations range from $-16.0°$ to $19.9°$. These values are comparable with the calculated values of the same boundary and other CSL boundaries in Si [11–15]. Large deviations are localised around the 5–7 units at the interface. The static charge fluctuations caused by the structural disorder are also localised in these structural units at the interface, and range from $-0.02e$ to $+0.02e$. These values are more reliable than those as large as $-0.14e$ in the calculation of the same boundary using the SETB method

without any form of self-consistency [11]. Correlation exists between the charge fluctuations and the structural disorder, although the precise relation between the respective charges of atoms and the local structural disorder is not clear. Excess electronic charges of $0.02e$ occur at atoms surrounded by bond-length shortening of 1.9% and 1.2%, although deficiencies of $0.02e$ also occur at atoms surrounded by bond-length shortening of 1.7% and 1.1%.

In the stable atomic configuration of the present boundary in SiC shown in figure 2, the bond-angle deviations range from $-23.1°$ to $24.1°$. The bond-length deviations of normal Si–C bonds range from $-2.5\%$ to $2.2\%$. Large deviations are also localised around the 5–7 units at the interface. The length of the Si–Si wrong bond is shorter by 4.3% than that in bulk Si and the length of the C–C wrong bond is longer by 3.8% than that in bulk diamond. As compared with the bond length in bulk SiC, the former is longer by 19.6% and the latter is shorter by 15.1%. Owing to the presence of these wrong bonds, the small rigid-body translation along the $[\bar{4}\bar{1}1]$ direction is introduced as mentioned above, and the deviations of bond angles and Si–C bond lengths are relatively large as compared with those in the boundary in Si. However, it can be said that the covalent bonds are well reconstructed at the interface in the present boundary of SiC as well as the case of Si.

In figure 2, large static charge fluctuations exist especially around the wrong bonds and are localised within several atomic layers at the interface. This indicates the importance of self-consistency. As compared with the perfect crystal, the largest deviation of electron occupancies of respective C atoms is a decrease of $0.14e$ at the C–C wrong bond and that of respective Si atoms is an increase of $0.20e$ at the Si–Si wrong bond.

Using the atomic structures and charge distributions shown in figures 1 and 2, the respective energy values in table 3 can be analysed. First, we analyse the energy values of Si. $E_{\rm pro}$ in Si includes the promotion energy and the change in the intra-atomic electrostatic energy between electrons as shown in equation (7*b*). The main reason for the increase of $E_{\rm pro}$ shown in table 3 is the increase of the s–p mixing around the interface, which is the ratio of p-orbital occupancy to s-orbital occupancy in the respective atoms [20]. The slight increase of total p-orbital occupancy in the present boundary structure causes the present increase of $E_{\rm pro}$. The changes in the intra-atomic electrostatic energy $\frac{1}{2}U_iQ_i^2$ of the respective atoms are small and counterbalanced to each other.

We have found fluctuations of the s–p mixing from $-0.014$ to $+0.024$ around the interface, and found a correlation between the s–p mixing and the bond-length deviations, although the correlation between the s–p mixing and the bond-angle deviations is not clear. As found in the case of the perfect crystals [20, 23], we have found that the bond-length shortening causes the increase of the s–p mixing. For example, the atom with effective charge $-0.02e$ has the maximum s–p mixing and is surrounded by the bond-length shortening of 1.9% and 1.2%. Inversely, the two atoms constituting the most lengthened bond have the smallest and second smallest values of s–p mixing. Around the interface of the present boundary structure in Si, there are many shortened bonds as compared with lengthened bonds, which causes the present increase of $E_{\rm pro}$. This is consistent with the negative value of $\Delta E_{\rm cov}$ and the positive value of $\Delta E_{\rm ov}$ in table 3.

$\Delta E_{\rm Mad}$ in Si is only a negligible contribution to the boundary energy as shown in table 3. This explains the fact that the values of grain boundary energy in Si calculated without any form of self-consistency [11, 15] are not so different from those of the present and other self-consistent calculations [12–14]. It seems that, at least in the structure where all the atoms are fourfold-coordinated, the self-consistency has a negligible effect in Si, as pointed out in [14].

The main contribution to the boundary energy in Si is the change in $E_{ov} + E_{cov}$, which is 1.583 eV per supercell. This is caused by structural disorder such as bond-length and bond-angle deviations. Of course, it is possible that the signs of $\Delta E_{ov}$ and $\Delta E_{cov}$ are inverted in defects such as those with many lengthened bonds, differently from the present boundary. The present method of calculation of $E_{ov}$ is much different from the SETB method [11]. However, the relatively small deviations of bond lengths in the present boundary result in a small difference between the calculated values of total boundary energy [11].

Then, we analyse the energy values of SiC in table 3. $\Delta E_{pro}$ is negative and relatively large, differently from that in Si. By analysing the charge fluctuations, it can be said that the reduction of the total intra-atomic electrostatic energy is most responsible for the present value of $\Delta E_{pro}$. The decrease of $Q_i$ at the C–C wrong bonds much reduces the total sum of $\frac{1}{2}U_iQ_i^2$ in $E_{pro}$ in spite of the increase of $Q_i$ at the Si–Si wrong bonds because $U_i$ is larger in C than in Si. This large reduction is counterbalanced by the following two effects and results in the present value of $\Delta E_{pro}$. First, the decrease of the total electron occupancy in C atoms and the increase of that in Si atoms caused by the wrong bonds contribute to the increase of $E_{pro}$ through the decrease of the energy gain by electron transfer from Si to C as compared with the perfect crystal. Secondly, slight increases of the s–p mixing occur in C atoms, especially at the wrong bonds. This contributes to the increase of $E_{pro}$.

There are also the fluctuations of the s–p mixing of respective atoms around the interface of the present boundary in SiC. The s–p mixing of C atoms at the C–C wrong bonds is increased as compared with that in the perfect crystal because of the shortened C–C bond length compared with the ordinary Si–C bond length. Inversely, the s–p mixing of the Si atoms at the Si–Si wrong bond is decreased because of the lengthened bond length. There is also a correlation between the s–p mixing and the lengths of the other Si–C bonds.

$\Delta E_{Mad}$ in the present boundary in SiC is relatively large because of the presence of the wrong bonds compared with that in Si. We have found that there are large deviations of the inter-atomic electrostatic potential (Madelung potential) for an electron, $P_i$ of equation (5), around the interface, especially at the wrong bonds, as well as charge fluctuations. In bulk SiC, $P_i$ at C atoms is negative and $P_i$ at Si atoms is positive. The absolute values of $P_i$ at the two C atoms of the C–C wrong bond are decreased by about 1.1 eV, and then the contributions to $\Delta E_{Mad}$, which is $\Delta\frac{1}{2}(Q_i - Z_i)P_i$, are +0.396 eV and +0.373 eV. At the two Si atoms of the Si–Si wrong bond, the absolute values of $P_i$ are decreased by about 1.2 eV and about 1.4 eV, and then the contributions to $\Delta E_{Mad}$ are +0.423 eV and +0.500 eV. These contributions of the atoms at the wrong bonds form 84% of $\Delta E_{Mad}$.

The deviations of $P_i$ larger than ±0.1 eV are concentrated in the region within about 4 Å from the interface. It is interesting that the directions of the deviations of $P_i$ in the two crystals on both sides of the interface are opposite to each other except for the boundary core region, in accordance with the absence of glide-plane symmetry in the present interface structure. In the upper crystal in figure 2, $P_i$ are all shifted in the negative direction, and in the lower crystal in figure 2, $P_i$ are all shifted in the positive direction. These small deviations of $P_i$ of respective atoms in the two crystals decrease slowly with increasing distances from the interface.

It should be noted that $\Delta E_{pro} + \Delta E_{Mad}$ is a large part of the boundary energy in SiC, differently from the case of Si. This is caused by the presence of the wrong bonds and is determined mainly by the intra-atomic and the inter-atomic electrostatic interactions.

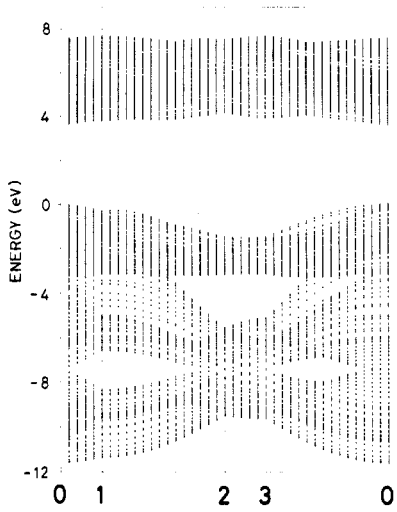


**Figure 3.** The energy band structure of the perfect crystal of Si. Points 0, 1, 2 and 3 in the Brillouin zone are $(0, 0, 0)$, $(\pi/R_1, 0, 0)$, $(\pi/R_1, \pi/R_2, 0)$ and $(0, \pi/R_2, 0)$, respectively, where $R_1 = (3\sqrt{2}/2)a_0$ and $R_2 = (\sqrt{2}/2)a_0$. In this notation, the $x$ axis is along the $[\bar{4}\bar{1}1]$ direction and the $y$ axis is along the $[0\,1\,1]$ direction. These are common in figures 4, 5 and 6.

This means the importance of self-consistency in treating lattice defects in solids with both covalent and ionic characters within the tight-binding theories, and it is important to treat both intra-atomic and inter-atomic electrostatic interactions self-consistently.

$\Delta E_{ov} + \Delta E_{cov}$ in SiC is 2.837 eV per supercell. This value is reasonable compared with the value of 1.583 eV in Si, considering the relation between the elastic properties of SiC and Si. It seems that the formation of wrong bonds does not affect $\Delta E_{ov} + \Delta E_{cov}$ so much compared with $\Delta E_{pro} + \Delta E_{Mad}$. In the formation of two Si–Si bonds and two C–C bonds from four Si–C bonds as well as the present supercell, the change in $E_{ov} + E_{cov}$ is estimated to be $-0.34$ eV from the values of the perfect crystals if all the bond lengths are the same as those in the perfect crystals [23]. (This indicates that $E_{Mad}$ is essential to stabilise SiC with respect to Si and C.) Therefore, the present value of $\Delta E_{ov} + \Delta E_{cov}$ is considered to be mainly caused by the bond distortions around the interface.

## 5. Electronic structure

Figures 3 and 4 show the electronic structures of the perfect crystal and the $\{1\,2\,2\}\,\Sigma = 9$ boundary in Si. Figures 5 and 6 show those in $\beta$-SiC. All these were calculated for the 144-atom cells, and those of the perfect crystals were calculated for supercells with the same size and the same periodicity as the supercells of the boundary. Results are shown along the lines in the plane with $k_z = 0$ in the orthorhombic Brillouin zone.

Here we should explain the electronic structures of the perfect crystals of Si and $\beta$-SiC given in the present theoretical scheme. The reproduction of the conduction bands of Si in the diamond structure and of SiC in the zincblende structure is poor, especially near the X and L points in the Brillouin zone, and the indirect band gap failed to be reproduced in Si and SiC, although the calculated values at the $\Gamma$ point are relatively correct. Thus the band gaps and the conduction bands are not correct in figures 3 and 5. This is a common drawback in the nearest-neighbour $sp^3$ tight-binding model, and can be improved by inclusion of excited atomic states in the basis set or inclusion of distant-neighbour matrix elements [24].

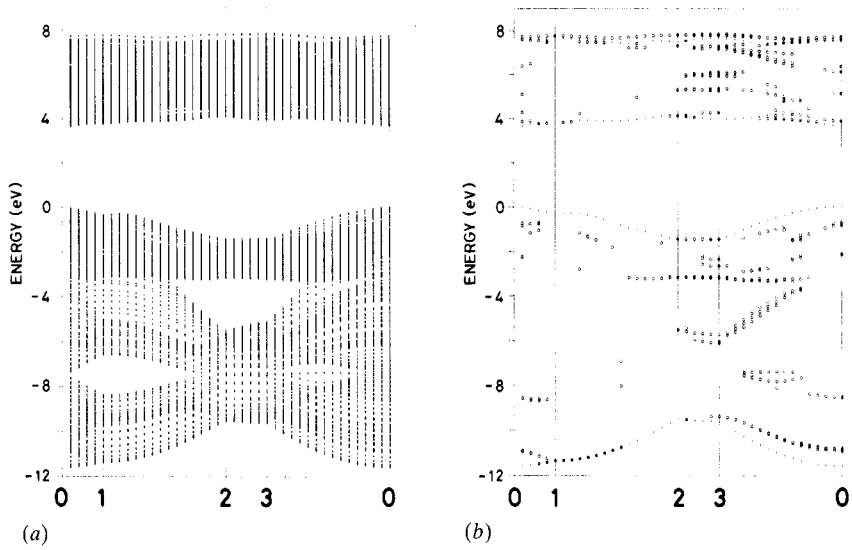


**Figure 4.** (*a*) The energy band structure of the {1 2 2} Σ = 9 grain boundary in Si. (*b*) Boundary-localised states. The states plotted are those for which the probability that an electron is located on the atoms of the 5–7 units at the interface exceeds 50%. The dotted curves indicate the bulk band structure of the perfect crystal.

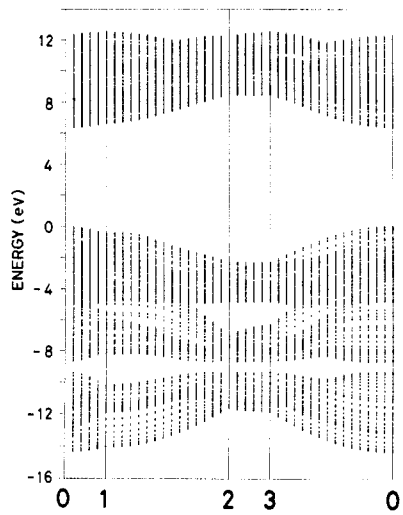


**Figure 5.** The energy band structure of the perfect crystal of β-SiC.

The valence band structure of Si is well reproduced using the present tight-binding parameters [21, 24]. However, the reproduction of that of β-SiC is only qualitative. Especially the total valence band width is underestimated by 25% compared with experiments and other theoretical calculations [26]. In order to obtain more quantitative results, it is necessary to use parameters fitted for SiC, differently from the present universal ones, as pointed out in our preceding paper [23].

Figure 4 shows the calculated electronic structure of the {1 2 2} Σ = 9 boundary in Si. Boundary-localised states are also shown. There are no deep states inside the

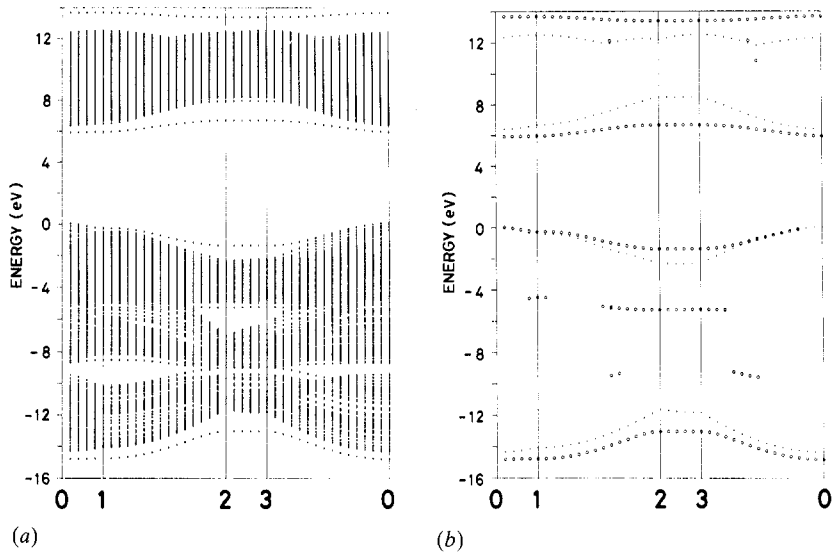


**Figure 6.** (*a*) The energy band structure of the {1 2 2} $\Sigma = 9$ grain boundary in $\beta$-SiC. (*b*) Wrong-bond localised states. The states plotted are those for which the probability that an electron is located on the atoms constituting the wrong bonds at the interface exceeds 25%.

fundamental gap in accordance with the smooth reconstruction of dangling bonds at the interface. However, boundary-localised states caused by structural disorder in the boundary core region are found at the band edges and within the bands. These features are similar to those found in the {2 1 1} $\Sigma = 3$ boundary and the {1 3 0} $\Sigma = 5$ boundary in Si in our previous calculations using the SETB method [15]. The states at $-7.8$ eV inside the pseudogap shown in figure 4 are most sharply localised, of which more than 90% of the contents are localised in the 5–7 units at the interface. These states are considered to be the same as those found in the calculation of the present boundary using the SETB method [11]. In the calculation using the density-functional theory [12], localised shallow states associated with the conduction band edge have been found. However, in the present calculation, such states do not exist although the presentation of the electronic states near the conduction band edge is not necessarily correct in the present scheme, as mentioned above.

Figure 6 shows the calculated electronic structure of the {1 2 2} $\Sigma = 9$ boundary in $\beta$-SiC. There are no deep states in the fundamental gap as well as the boundary in Si. However, it is remarkable that many new states occur especially at the band edges as compared with that of the perfect crystal in figure 5. As shown in figure 6(*b*), most of these new states are associated with the wrong bonds at the interface. New bands at the top of the valence band and at the bottom of the conduction band are localised states at the Si–Si wrong bonds. Especially, the states below the bulk conduction band edge near the points 2 and 3 are sharply localised, of which more than 90% of the contents are localised at the Si–Si wrong bonds and neighbouring atoms in the 5–7 units at the interface. New bands at the bottom of the valence band and above the conduction band are localised states at the C–C wrong bonds. All these states are sharply localised, of which more than 90% of the contents are localised at the C–C wrong bonds and neighbouring atoms in the 5–7 units at the interface. Also localised states at the C–C wrong bonds exist near the pseudogaps within the valence band. States sharply localised

not to the wrong bonds but to the 5–7 units themselves also exist at the lower edge of the bulk conduction band edge along the line from point 2 to point 3 in figure 6(*a*) as compared with figure 5.

Of course, it should be noted that these results are qualitative and the eigenenergies are not necessarily correct, especially around the conduction band, as mentioned above. However, it is remarkable that the wrong bonds cause sharply localised states in the present boundary in SiC as compared with the boundary in Si. Especially, the Si–Si wrong bonds induce localised states inside the gap. However, these states are shallow states and it can be concluded that the present boundary in SiC is electrically non-active as well as reconstructed boundaries in Si.

The mechanism of the occurrence of these wrong-bond localised states is analysed as follows. The electronic structure depends on the final self-consistent form of the Hamiltonian. The changes in the inter-atomic matrix elements $H_{\alpha\beta}(\boldsymbol{t}_i, \boldsymbol{t}_j + \boldsymbol{R})$ caused by the large deviations of the bond lengths of the wrong bonds as compared with the bulk Si–C bonds are most important. At the C–C wrong bonds, the bond length is shortened by 15.1% as compared with the bulk Si–C bond length. This results in an increase of 39% in the magnitude of the inter-atomic matrix elements. At the Si–Si wrong bonds, the bond length is lengthened by 19.6% and this results in a decrease of 30% in the magnitude of the inter-atomic elements. From the viewpoint of the bond orbital model [27], bonding and antibonding states, between which the splits are large because of the large magnitude of the matrix elements, are formed between the C atomic orbitals of low energy levels at the C–C wrong bonds. At the Si–Si wrong bonds, bonding and antibonding states, between which the splits are small because of the relatively small magnitude of the matrix elements, are formed between the Si atomic orbitals of high energy levels. It can be said that the former two types of states are the origin of the C–C bond localised states at the bottom of and within the valence band and those above the conduction band, respectively. It can also be said that the latter two types of states are the origins of the Si–Si bond localised states at the top of the valence band and those at the bottom of the conduction band, respectively.

The changes in the on-site elements $E_{i\alpha}$ at the wrong bonds themselves are relatively small. It is the fourth term in equation (3), the non-orthogonality correction, that most affects the on-site elements at the wrong bonds. Of course, the intra-atomic electrostatic potential, $U_i(Q_i - Z_i)$, and the inter-atomic electrostatic potential, $P_i$, in equation (3), are much changed at the sites of the wrong bonds, as mentioned above. However, the changes in these two terms are opposite, counterbalanced to each other, and do not affect the on-site elements themselves so much. This explains the empirical success of electronic structure calculations of lattice defects in compounds in usual tight-binding theories using fixed on-site elements [28]. However, it should be noted that this is the case in calculation of eigenenergies. In calculation of total energies, the self-consistency including the intra-atomic and inter-atomic electrostatic interactions is important, as shown in the preceding section.

In this way, it can be said that the present results of the electronic structure of the $\{1\,2\,2\}\,\Sigma = 9$ boundary in SiC are rather general. On the other hand, it has been pointed out that wrong bonds in amorphous III–V or II–VI compound semiconductors frequently cause mid-gap states [28]. These states have characters of the bonding states between cations and the antibonding states between anions. The reason why the wrong bonds do not cause deep states in the present case is that the differences between the atomic levels of C and Si are not so large as compared with compound semiconductors. The present result is consistent with the calculations of antisite defects in cubic SiC [29, 30], where

no states in the fundamental gap were found, differently from the case of the III–V compound semiconductors.

## 6. Conclusions

We have calculated the boundary energy, the stable atomic configuration and the electronic structure of the $\{1\,2\,2\}\,\Sigma = 9$ boundary in $\beta$-SiC quantum-mechanically for the first time. We have constructed an atomic model of this boundary in $\beta$-SiC consisting of a zig-zag arrangement of 5–7 units similar to that in the same boundary in Si from a HREM image, although Si–Si and C–C wrong bonds are repeated alternately at the interface in this model. We have used the SCTB method. This method can treat both covalency and ionicity on an equal footing and can incorporate the effects of self-consistent charge redistribution and intra-atomic and inter-atomic electrostatic interactions. These effects have been shown to be essential in calculations of the boundary energy in SiC.

We have also performed similar calculations of the same boundary in Si for comparison. The calculated results for Si have shown the stability and the electrical non-activity of the present boundary structure in Si similarly to the results obtained using the SETB method and the density-functional theory. From the analysis of the respective energy terms in the SCTB method, it seems that self-consistency is a negligible effect in Si, at least in structures where all the atoms are fourfold-coordinated.

From the calculated boundary energy in SiC, we can conclude that the present reconstructed atomic model can exist stably as compared with the surface energies. The calculated boundary electronic structure in SiC has no deep states in the fundamental gap and it can be said that the present boundary structure in SiC is electrically non-active as well as the same boundary in Si, although the wrong bonds introduce the wrong-bond localised states at the band edges and within the valence band.

Of course, it is necessary to examine other atomic models containing only one type of wrong bonds as mentioned in section 2, and further experimental observations are needed in order to decide on the structure really existing at the $\{1\,2\,2\}\,\Sigma = 9$ boundary in $\beta$-SiC. The remarkable features of the present structure obtained by the calculation as compared with other models are a small rigid-body translation along the $\langle 4\,1\,1\rangle$ direction and the opposite deviations of Madelung potentials at respective atoms in the two grains on both sides of the interface because of the absence of glide-plane symmetry at the interface.

In any case, the present results indicate that structural units such as five-membered rings and seven-membered rings can exist stably and cause no deep states in grain boundaries in SiC as well as in Si. This means the possibility that electrically non-active and atomistically reconstructed boundaries can be constructed in general by arranging structural units, in SiC as well as in covalent semiconductors. This is consistent with the observations of the coherent matching between adjoining grains in other types of boundaries in SiC [1, 4].

However, the effects of the wrong bonds in boundaries in SiC are important. The increase in the electrostatic energy caused by the wrong bonds at the interface is a large part of the present boundary energy in SiC, differently from that in Si, and it has been found that the wrong bonds at the interface introduce the wrong-bond localised states at the band edges and within the valence band. It is possible that energies and electronic structures of boundaries in SiC are much influenced by the numbers and kinds of wrong bonds at interfaces. Thus it might be possible that there exist boundary structures of

SiC fairly different from those in covalent semiconductors in order to decrease the electrostatic energy associated with wrong bonds. It seem that the effects of impurities can be analysed with respect to the wrong bonds. For example, there may be the possibility that impurity atoms such as oxygen can easily intervene between Si atoms at the Si–Si wrong bonds in general boundaries in SiC.

## Acknowledgments

We would like to thank Professor K Hiraga and Dr S Hagège for valuable information about the HREM image and recent image simulation. All the calculations were performed on the CRAY X-MP at RIPS Center of the Agency of Industrial Science and Technology. We would like to thank the staff of RIPS Center for their help in using the supercomputer.

## References

[1] Hiraga K 1984 *Sci. Rep. Res. Inst. Tohoku Univ.* A **32** 1
[2] Thomas G 1987 *Materials Science Research* vol 21, ed J A Pask and A G Evans (New York: Plenum) p 55
[3] Merkle K L, Reddy J F, Wiley C L and Smith D J 1987 *Materials Science Research* vol 21, ed J A Pask and A G Evans (New York: Plenum) p 241
[4] Ichinose H, Inomata Y and Ishida Y 1987 *Materials Science Research* vol 21, ed J A Pask and A G Evans (New York: Plenum) p 255
[5] Wolf D 1984 *J. Am. Ceram. Soc.* **67** 1
[6] Duffy D M 1986 *J. Phys. C: Solid State Phys.* **19** 4393
[7] Stoneham A M and Tasker P W 1987 *Materials Science Research* vol 21, ed J A Pask and A G Evans (New York: Plenum) p 155
[8] Krivanek O L, Isoda S and Kobayashi K 1977 *Phil. Mag.* **36** 931
[9] d'Anterroches C and Bourret A 1984 *Phil. Mag.* A **49** 783
[10] Bourret A and Bacmann J J 1985 *Surf. Sci.* **162** 495
[11] Thomson R E and Chadi D J 1984 *Phys. Rev.* B **29** 889
[12] DiVincenzo D P, Alerhand O L, Schlüter M and Wilkins J W 1986 *Phys. Rev. Lett.* **56** 1925
[13] Paxton A T and Sutton A P 1988 *J. Phys. C: Solid State Phys.* **21** L481
[14] Paxton A T and Sutton A P 1989 *Acta Metall.* **37** 1693
[15] Kohyama M, Yamamoto R, Ebata Y and Kinoshita M 1988 *J. Phys. C: Solid State Phys.* **21** 3205
Kohyama M, Yamamoto R, Watanabe Y, Ebata Y and Kinoshita M 1988 *J. Phys. C: Solid State Phys.* **21** L695
[16] Papon A M and Petit M 1985 *Scr. Metall.* **19** 391
Kohyama M, Yamamoto R and Doyama M 1986 *Phys. Status Solidi* b **137** 11
[17] Hagège S, Shindo D, Hiraga K and Hirabayashi M 1990 *Proc. Int. Congr. on Intergranular and Interphase Boundaries in Materials* (Les Ulis, France: Les Editions de Physique) p 167
[18] Pond R C and Vlachavas D S 1983 *Proc. R. Soc. Lond.* A **386** 95
[19] Chadi D J 1978 *Phys. Rev. Lett.* **41** 1062; 1984 *Phys. Rev.* B **29** 785
[20] Paxton A T, Sutton A P and Nex C M M 1987 *J. Phys. C: Solid State Phys.* **20** L263
Sutton A P, Finnis M W, Pettifor D G and Ohta Y 1988 *J. Phys. C: Solid State Phys.* **21** 35
[21] Majewski J A and Vogl P 1987 *Phys. Rev.* B **35** 9666
[22] Kohyama M, Yamamoto R, Ebata Y and Kinoshita M 1989 *Phys. Status Solidi* b **152** 533
[23] Kohyama M, Kose S, Kinoshita M and Yamamoto R 1990 *J. Phys.: Condens. Matter* **2** 7791
[24] Vogl P, Hjalmarson H P and Dow J D 1983 *J. Phys. Chem. Solids* **44** 365
[25] Takai T, Halicioğlu T and Tiller W A 1985 *Surf. Sci.* **164** 341
[26] Hemstreet L A Jr and Fong C Y 1971 *Solid State Commun.* **9** 643; 1972 *Phys. Rev.* B **6** 1464
[27] Harrison W A 1980 *Electronic Structure and the Properties of Solids* (San Francisco: Freeman)
[28] O'Reilly E P and Robertson J 1986 *Phys. Rev.* B **34** 8684
[29] Li Y and Lin-Chung P J 1987 *Phys. Rev.* B **36** 1130
[30] Wang C, Bernholc J and Davis R F 1988 *Phys. Rev.* B **38** 12752